metals

MDPI

Article

Comparative Analysis of the Stainless Steel Mesh Size Effect on Oil–Water Emulsion Separation with and Without Ni Coating

Mohanad Khairi [1,2,*] and Peter Baumli [1]

[1] Institute of Metallurgy, Metal Forming and Nanotechnology, University of Miskolc, 3515 Miskolc, Hungary; peter.baumli@uni-miskolc.hu
[2] Inspection Engineering Department, Midland Oil Company, Ministry of Oil, Baghdad 10064, Iraq
* Correspondence: mohanad.khairi@uni-miskolc.hu or mohnad_alasdi@yahoo.com

Abstract

Oil–water separation is of enormous importance because it has practical implications for addressing corrosion problems in the oil industry, arising from direct contact between the inner surfaces of pipelines and water containing oil. Therefore, the development of functional materials for handling oil–water mixtures is crucial and has significant economic benefits in the future. Using metal meshes remains a complex process because the properties of the extracted oil mixture (emulsion) vary across fields, which can affect the efficiency of the separation process and the required mesh size for optimal results. Still, it is considered a promising approach for separation. In this study, stainless steel meshes of various mesh sizes (180, 200, 300, 400, and 500 meshes) were coated with a 0.1-micron-thick layer of nickel by physical vapour deposition (PVD). The separation efficiency of stainless steel meshes, both with and without Ni coating, was examined at room temperature using an emulsion (50% vol. petroleum and 50% vol. water) prepared in the laboratory. The Ni-coated meshes achieved high separation efficiencies of 97% and 92% for mesh sizes 400 and 300, respectively. An 8% increase in the separation efficiency of the 200 mesh size resulted in about 80% efficiency with a Ni coating. Hence, it can be concluded that the prepared meshes have potential for high-efficiency oil–water separation, which may help reduce water transport to subsequent processing stages and mitigate corrosion-related issues.

Keywords: oil–water separation; Ni coating; stainless steel meshes; anti-corrosion; wettability; oil pipelines

1. Introduction

The process of extracting oil from the ground remains affected by the amount of water accompanying the oil, which in turn affects the pipes, which suffer from different types of internal corrosion (including stress-orientated hydrogen-induced, hydrogen-induced lamination, top-of-line corrosion, pitting, hydrogen-induced cracking, mesa attack, stepwise cracking, hydrogen blistering, under-deposit corrosion, girth weld, sulphide stress cracking, stress corrosion cracking, and preferential weld corrosion) due to the water accompanying the oil [1–7], thus affecting the quality, quantity, and production rate, resulting in economic losses due to shutdown and maintenance. Additionally, the environmental impact cannot be overlooked [8]. Here, it was necessary to identify modern, practical, effective, economical, and long-lasting methods that can be easily used to separate water from oil during the first extraction process to avoid or reduce its effects to the lowest possible level.

Check for updates

Academic Editor: Branimir N. Grgur

Received: 28 April 2026
Revised: 1 June 2026
Accepted: 2 June 2026
Published: 5 June 2026

Copyright: © 2026 by the authors. Licensee MDPI, Basel, Switzerland. This article is an open access article distributed under the terms and conditions of the Creative Commons Attribution (CC BY) license.

Oil–water separation techniques are classified into filtration methods (membrane, filter, film, and mesh) and absorbent materials (porous media, powders/particles, gels, and nanocomposites) [9]. These methods have been used in many applications (including cleaning oil spills in rivers and seas, purifying water from oils for industrial, medical, and human uses, or separating water from oil at different stages of the oil industry) [10]. The working principle of these applications depends on differences in the wetting behaviour of oil and water on metal surfaces, which are classified as oleophilic and hydrophobic [11]. Consequently, stainless steel meshes are used to separate oil from water, allowing oil to pass through while preventing water from penetrating [12].

There are many challenges [13–17] that have been faced the separation process by meshes during the initial use of metal meshes for oil–water separation without any coatings, which suffered from low corrosion resistance, especially when exposed to the hard environments typically encountered in oil–water separation processes (salty water, acidic, or basic conditions), and early designs did not incorporate self-cleaning features or materials resistant to the adhesion of contaminants (which reduced their effectiveness and required frequent cleaning or replacement), or they were not durable enough to withstand the high pressures or mechanical stresses of industrial applications (leading to deformation or failure during use). Additionally, the costly production and rough structures limited use in a different applications due to lower lifetime use and performance limitations.

Initially, control of these challenges was achieved using metal meshes of different sizes, which directly affect hole dimensions [18–20] and play an essential role in determining separation efficiency, production rate, and selectivity through their interaction with wettability behaviour. Recent developments in surface modification technologies have enabled these meshes to selectively separate oil from water or vice versa, depending on specific application requirements, such as hydrophilic or oleophilic. Therefore, researchers [21–28] sought to develop alternative solutions to enhance separation and extend the lifespan of metal meshes by coating their surfaces, thereby improving durability and hardness. These coatings include immersion in fatty acid solutions, electrodeposition, chemical modification with low-surface-energy materials, electroless galvanic deposition, electroplating, etching, sandblasting, solution immersion, and spray and dry.

On the other hand, many researchers used different types of coating to improve oil–water separation by stainless steel mesh, including one-layer silica-coated stainless steel mesh [29], double-layer modified silica-coated stainless steel mesh [30], the atomic layer deposition method to deposit TiO_2 [31], and a hydrothermal synthesis method used to deposit TiO_2 coating [13].

Seongjae Myeong et al. [32] prepared a hydrophobic mesh filter using carbon coating and fluorine plasma treatment by physical vapour deposition (PVD) to achieve uniform nanoscale coating. The PVD carbon coating increased hydrophobicity, with a contact angle of 120°. However, the study leaves a gap in understanding how mesh filter efficiency will change across different types of oils with properties similar to crude oil; it focused on a specific type of oily wastewater (soybean oil).

One promising approach involves the method of selecting the metal type used in coating stainless steel meshes based on Equations (1) and (2) developed to predict the wettability behaviour of metals [11], which was proved according to Becker's broken bond model [33,34].

For petroleum (apolar):

$$\cos\theta = -p\,r + 1 \quad (1)$$

For water (polar):

$$\cos\theta = p\,r - 1 \quad (2)$$

where θ is the contact angle, r is the metal atomic radius in pm, p is the semi-empirical parameter for petroleum, 0.00068 (1/pm), and water is 0.0089 (1/pm).

In this study [11], the researchers applied the broken bond model to describe more precisely the wettability behaviour in wettability tests for polar and apolar liquids, where they proved that the linear relationship between the cosine of the contact angle ($\cos\theta$) and the atomic radius of a metal is derived from how the atomic radius affects the surface energy and, consequently, wettability, where the separation opportunity will be increased when decreasing the atomic radius of a metal.

Based on Equations (1) and (2), we can select Ni to enhance separation and impart superhydrophobic (water-repelling) and oleophilic (oil-attracting) properties to the stainless steel meshes after coating. In addition to chemical stability and mechanical strength, where many studies [35–38] proved Ni coatings allow for the creation of micro- and nanoscale surface structures that optimise their wettability and highlight that the hierarchical structure (multilevel structural arrangement) formed by nickel coatings significantly improves the long-term durability and reusability of the meshes, making them suitable for continuous industrial applications, they did not discover the separation efficiency when using emulsion or study the effect of differences in hole mesh size on the separation efficiency.

Other researchers enhanced the Ni coatings on stainless steel mesh using different methods, such as electrochemically depositing a layered double hydroxide (LDH) by Liu [39]. The preparation took only a few minutes and greatly improved production efficiency, as well as the positive charge of LDH, which promotes the rupture of emulsion droplets and improves emulsion separation efficiency. Hou et al. [40] prepared nickel-coated meshes via electrodeposition in a deep eutectic solvent (DES) composed of choline chloride (ChCl) and ethylene glycol (EG), and the resulting meshes exhibited superior chemical stability in acidic, alkaline, and salt solutions.

In practical applications, mesh contamination can reduce separation efficiency by accumulating suspended particles, waxes, salts, and other contaminants on the mesh surface. Several mitigation approaches can be employed, including periodic cleaning, pre-filtration, optimisation of mesh size, flow rate control, and the development of anti-contamination surface modifications. The Ni coating may also help reduce contaminant adhesion due to its selective wettability [40].

This study evaluates differences in emulsion (petroleum–water) separation efficiency between stainless steel meshes with different sizes (180, 200, 300, 400, and 500 meshes), both coated and uncoated with PVD nickel. Verifying the emulsion separation efficiency involves a new method that depends on the carbon content. The primary aim is to explore the hydrophobicity and oleophilicity behaviour of stainless steel meshes with and without Ni coating, determine their separation efficiencies, and determine the optimal stainless steel mesh hole size for the emulsion separation process. Additionally, to assess their mechanical stability and reusability in repeated use cycles. The findings are expected to contribute to the robust development of economic, high-performance separation technologies for environmental and industrial applications.

2. Materials and Methods

2.1. Materials

In the experiment part, firstly, we used two substrates of pure nickel and stainless steel (97.8 wt.% Fe, 1.9 wt.% Mn, 0.48 wt.% C, 0.35 wt.% Si, 0.035 wt.% P, and 0.04 wt.% S) to measure the contact angle of water using the sessile drop method on air and under petroleum to prove the differences in water wettability behaviour in the two environments (see Section 2.3.1). The main samples for the separation process were the meshes (Tables 1 and 2) made of stainless steel with different sizes (500, 400, 300, 200, and 180 meshes) and pur-

chased from Putian Xinyu District Blue Sky Electronic Commerce Co., Ltd. (Fujian, China) and Yiwu Huili Metal Product Firm Co., Ltd. (Yiwu, China). The hole and wire diameters of the stainless steel mesh were determined from manufacturer specifications and verified by microscopic observation. The elemental compositions were obtained via EDS analysis and are presented only to confirm the general austenitic stainless steel composition of the investigated meshes. The stainless steel surface was coated with Ni by PVD (see The PVD Coating section). In my experiment, we investigated the coated and uncoated meshes as well (see Section 2.4) with two types of liquids. First, distilled water was mixed with a 0.02 g red-colored food powder (E514 sodium sulphate + E122 carmoisine) from Vora Spices Mills LLP, Mumbai, India, before being combined with the petroleum, or it was used in contact angle measurements, allowing it to clarify the difference between water behaviour and petroleum under petroleum or/and after separation. The second liquid is refined petroleum (MOL Group) (88–92 wt.% hydrocarbon, C10–C13, n-alkanes, iso-alkanes, cyclic compounds, <2% aromatics; 8–12 wt.% hydrocarbon, C15–C20, n-alkanes, iso-alkanes, cycloalkanes, <0.03% aromatics; and 8–12 wt.% hydrocarbon, C15–C20, n-alkanes, iso-alkanes, cycloalkanes, <0.03% aromatics), with the properties of petroleum (density = 0.760 g/cm^3 and viscosity = 6.21 Pa·s), and distilled water (density = 0.9982 g/cm^3 and viscosity = 1.0034 Pa·s). We used these two liquids to prepare emulsions with different compositions; the preparation details are in Section 2.2.2.

Table 1. The properties of the stainless steel mesh samples.

No.	Mesh Size	Hole Diameter mm	Wire Diameter mm
a	500	0.026	0.0254
b	400	0.033	0.0254
c	300	0.040	0.0381
d	200	0.080	0.0533
e	180	0.082	0.08

Table 2. The chemical composition of the stainless steel mesh samples without coating.

No.	Mesh Size	wt.% Fe	wt.% Cr	wt.% Ni	wt.% Other Elements
a	500	68.31	18.33	11.54	1.82
b	400	68.63	18.40	11.12	1.85
c	300	68.89	18.45	11.16	1.50
d	200	73.33	19.41	7.26	-
e	180	73.88	18.62	7.50	-

2.2. Preparation of the Samples

2.2.1. Stainless Steel Mesh Preparation

Cutting, Cleaning, and Fixing

The meshes were cut into square shapes with a size of 10 mm × 10 mm; they were ultrasonically treated in 0.1 M H_2SO_4 solution and ethanol, respectively, for 5 min to remove any organic impurities and prevent unwanted side reactions or any changes to surface chemistry during the experiment. Then, we ensured the reproducibility and consistency of the results. Under room temperature (~25 °C), they were dried. After that, the meshes were fixed to the handmade wooden frame to keep the plane level (Figure 1).

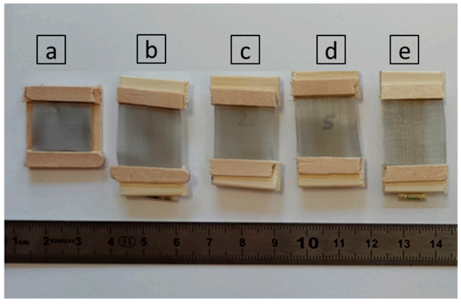


Figure 1. Fixation of the stainless steel meshes (a: 500, b: 400, c: 300, d: 200, e: 180 mesh sizes) without Ni coating.

The PVD Coating

As we mentioned in Section 2.1, the meshes were coated with Ni; in this chapter, we provide details of the Ni coating process. A 0.10 µm layer of Ni coating was deposited when the meshes were static in front of the target in an argon atmosphere using a DC magnetron sputtering PVD technique. The samples were fixed on a plate and then inserted into the upper device chamber, while the Ni target (diameter 50 mm and thickness 3 mm) was fixed in the shutter, which was operated under negative cathodic bias during DC magnetron sputtering. The deposition parameters were chamber pressure = 5.7×10^{-3} mbar, argon = 90 sccm, voltage = 250 V, and current = 250 mA (voltage and current are the sputtering power supply operating conditions applied to the Ni target during deposition), the temperature was ~25 °C, and the tooling factor = 100 (this parameter is used to correct the thickness measured by the quartz crystal monitor (QCM) to match the actual thickness deposited on the substrate). The PVD device was from the Korvus Technology company (High Wycombe, London, UK), and the Niobium software version 2.0.0.196 interface was used to control the process and its parameters.

2.2.2. Preparation of the Petroleum–Water Emulsion

To mix petroleum with water, it was necessary to use stabiliser powders, like cetyltrimethylammonium bromide (CTAB), because these are often employed in petroleum–water mixtures (emulsions) to maintain stability and prevent the separation of petroleum and water phases. Stabilisers help maintain the dispersed phase (petroleum or water) within the continuous phase by reducing interfacial tension, forming a protective barrier around droplets and preventing dispersed droplets from merging into larger ones, which could lead to separation. This means stabilisers maintain homogeneity, prevent sedimentation or creaming, and ensure the long-term stability of the emulsion during the experiment. A total of 0.1 g of CTAB powder was added to 100 mL of water, and the mixture was shaken by hand to ensure mixing. This solution was used in the experiment and mixed with petroleum to form an emulsion as follows:

a. First, to establish a calibration standard for evaluating the separation results later, five mixtures with known volume ratios were prepared of petroleum–water mixing (20% petroleum + 80% water; 35% petroleum + 65% water; 50% petroleum + 50% water; 65% petroleum + 35% water; and 80% petroleum + 20% water) in addition to 100% petroleum and 100% water. Then, they were analysed using an elemental analyser EA1108, from Carlo Erba Instruments (Milan, Italy), and the hydrocarbon ratios for each sample were calculated using Clarity software version 8.8.1.1.6.
b. Equal proportions of (50% vol.) water and (50% vol.) petroleum were mixed for use in a main phase separation experiment (see Section 2.4).

2.3. Contact Angle Measuring

The sessile drop and captive bubble techniques were employed to determine the contact angle. Using an automatic pipette, 5 µL of the required liquid was placed separately on the surface of a cleaned substrate for 5 min per sample, and a CCD camera was used to record changes in the silhouettes of the formed drops. The CCD camera is connected to a computer running KSV software version 4.00 (CAM2008, KSV Instruments Ltd., Helsinki, Finland) to determine the contact angle. The experiments were conducted at room temperature (~25 °C), and the contact angle was measured repeatedly (about 10 times) for each sample. The experimental procedures were conducted using the sessile drop technique, utilising equipment developed by Sunplant Ltd. (Miskolc, Hungary) [11].

2.3.1. Water Contact Angle Measuring in Air and Petroleum Phase

The contact angle of water was determined using the sessile drop method on both nickel and stainless steel surfaces, which were initially placed separately in a container under two distinct environments; first, in ambient air, and second, in a petroleum phase, enabling a comparative analysis of wettability in the two environments on different metal surfaces. A 5 µL droplet of colored distilled water was placed onto each surface; the contact angle was then measured under air conditions (Figure 2a). Subsequently, for the measurements in petroleum, the solid substrates were first immersed in petroleum, after which a 5 µL droplet of colored distilled water was carefully deposited onto the submerged surface (Figure 2b,c).

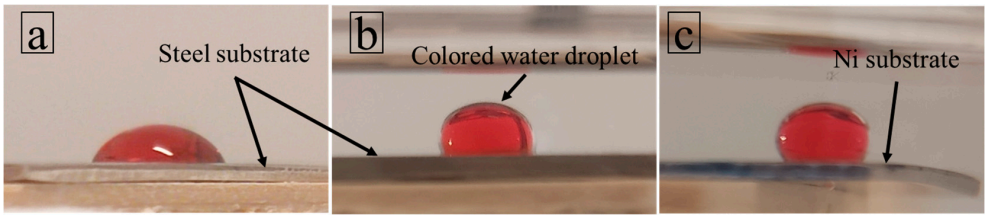


Figure 2. The wettability behaviour of a water droplet ((**a**) stainless steel substrate in air, (**b**) stainless steel substrate under petroleum phase, (**c**) Ni substrate under petroleum phase).

2.3.2. Petroleum and Water Contact Angles Measured on the Stainless Steel Mesh Surface Without and with Ni Coating

To simulate the results proven by [11,41] and provide an understanding of the wetting characteristics of liquids (petroleum and water) and the possibility of applying this behaviour to stainless steel mesh surfaces, the measuring techniques described were employed to determine the contact angle of 5 µL drops of distilled water and petroleum, which were placed separately on the surface of cleaned meshes (without and with Ni coating) for 5 min for each sample (Figure 3). Later, the actual separation experiments will be performed using these stainless steel meshes (without and with Ni coating) (see Section 2.4).

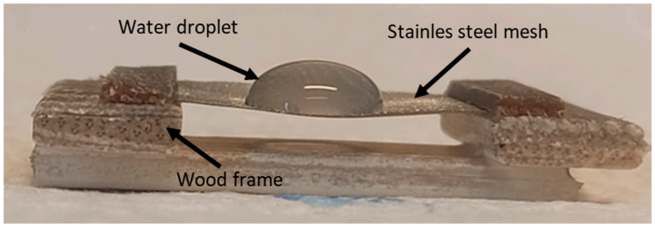


Figure 3. The wettability behaviour of a water droplet on the stainless steel mesh (300 mesh size) surface with Ni coating.

2.4. The Separation Process and Investigation

In the present study, to evaluate the emulsion (petroleum–water) separation ability with the prepared meshes (coated and uncoated by Ni), we isolate and evaluate the influence of stainless steel mesh size and Ni coating on separation efficiency under controlled laboratory conditions; therefore, the other parameters were intentionally kept constant throughout all experiments to ensure a reliable comparison between coated and uncoated meshes. All the emulsion separation experiments were conducted at room temperature (~25 °C) and under normal atmospheric pressure. Using a laboratory pipette, an amount of 20 µL droplet volume of the previously prepared fixed emulsion (50% vol. water + 50% vol. petroleum) with the same stabiliser concentration (CTAB) (as mentioned in Section 2.2.2, point b) was placed on the stainless steel mesh surfaces that the holder fixed (Figure 4). After one minute of the equilibrium state, the petroleum began to pass through the mesh and collect at the bottom of the container. The petroleum–water separation process was repeated 10 times for each stainless steel mesh, both with and without a Ni coating.

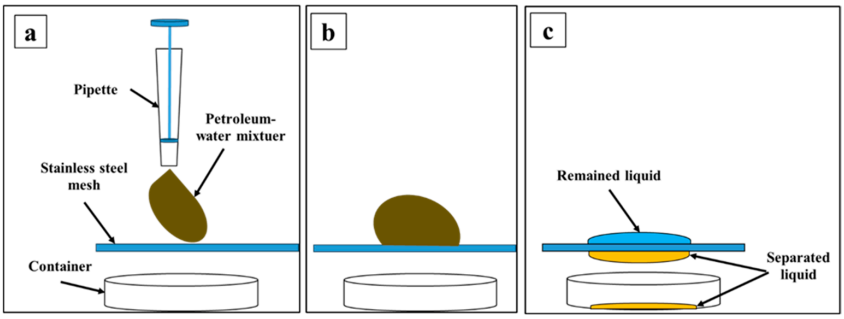


Figure 4. Schematic diagram of the emulsion (petroleum–water) separation process using stainless steel meshes coated and uncoated with Ni ((**a**) placement of the emulsion droplet on the stainless steel mesh surface; (**b**) equilibrium phase; (**c**) separation).

Only the liquid that separates under the mesh is collected using a pipette for examination and calculation of the hydrocarbon content percentage. After separation, small laboratory capsules are filled with the separated liquid, and the weight of each quantity in the capsule is measured with an accurate electronic balance. The weighed and numbered capsules were transferred and placed into the holes of a rotating disc, which causes them to fall into the Element Analyser device (Milan, Italy) in sequence after each analysis of the previous capsule. The Element Analyser device is connected to the computer, from which the Clarity program software will collect and detail the results by sample number.

3. Results and Discussion

3.1. Water Droplet Wetting Behaviour Under the Petroleum Phase

The contact angle measurements on the nickel substrate reveal a distinct change in wettability with the surrounding medium. In ambient air, the water droplet exhibited a contact angle of $\theta = 77 \pm 5^{\circ}$ (Figure 5a), indicating a moderately hydrophilic surface with partial wetting behaviour. Similar contact angle ranges for untreated or naturally oxidised nickel surfaces have been widely reported in the literature, with the native oxide/hydroxide layer contributing to moderate hydrophilicity through polar interactions with water molecules [42,43]. In contrast, when the measurement was conducted in a petroleum environment, the apparent contact angle of the water droplet increased significantly to $\theta = 147 \pm 5^{\circ}$ (Figure 5b), reflecting a transition to a non-wetting, or effectively hydrophobic, state. This value is particularly significant because it approaches the superhydrophobic regime reported in advanced engineered systems, despite the absence of complex hierarchical texturing or fluorinated surface treatments, which are commonly re-

quired in previous studies [44,45]. The result obtained, therefore, demonstrates that highly effective wettability alteration can be achieved through comparatively simple modifications of metallic surfaces and interfacial adsorption mechanisms.

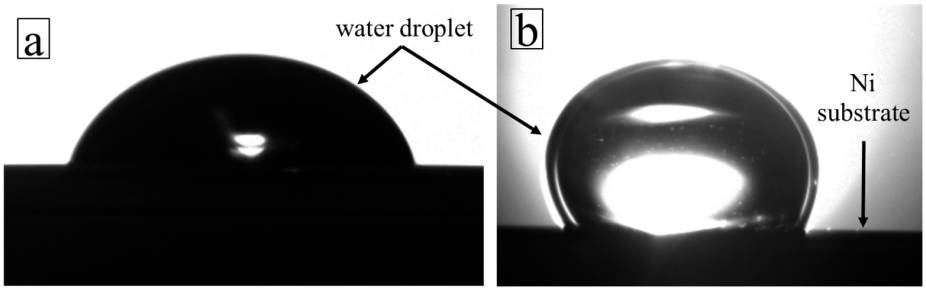


Figure 5. The silhouette of the water droplet on a nickel substrate surface ((**a**) in air, (**b**) under a petroleum phase).

This increase in contact angle can be attributed to the altered interfacial energy balance at the solid–liquid–liquid interface, where the petroleum phase modifies the interfacial tension balance within the solid–water–petroleum system, resulting in reduced water wettability and a higher apparent contact angle under submerged conditions, promoting the formation of a more spherical droplet morphology. Comparable wettability transitions have been reported for metallic and mineral substrates exposed to hydrocarbon-rich environments; however, the magnitude of the contact angle increase observed in the present study is notably larger than that reported for many conventional untreated metallic systems [46,47]. These results suggest that the present Ni surface exhibits particularly favourable interfacial selectivity toward petroleum-rich phases.

Furthermore, the presence of this adsorbed hydrocarbon layer suppresses polar interactions between water and the native nickel oxide, thereby increasing the solid–water interfacial energy. This layer reduces the work of adhesion between water and the surface, further contributing to the observed non-wetting behaviour. A similar reduction in water affinity due to hydrocarbon adsorption has been reported for several metallic and oxide surfaces [45]; however, the present study demonstrates that substantial wettability alteration can occur even on relatively simple PVD-modified Ni surfaces, highlighting the strong effectiveness of the deposited coating and the petroleum–surface interfacial interactions.

The steel surface exhibits a contact angle of approximately 59 $\pm$ 5° in air (Figure 6a), indicating a more pronounced hydrophilic character than that of nickel. This behaviour is primarily attributed to the presence of a native iron oxide/hydroxide layer on steel, which is highly polar and can form favourable interactions (e.g., hydrogen bonding) with water. Similar contact angle values have been reported for oxidised steel surfaces in previous wettability studies [48]. Nevertheless, when immersed in petroleum, the apparent contact angle increased significantly to approximately 95 $\pm$ 5° (Figure 6b), indicating a clear transition toward non-wetting behaviour. Although this value is lower than that obtained for nickel, it still represents a substantial wettability shift compared with many previously reported untreated steel systems, where only moderate contact angle changes were observed after petroleum exposure [44,46].

From a separation perspective, this contrast of wettability is highly advantageous. The relatively higher contact angle of water under petroleum implies that water droplets experience reduced adhesion to the metal surfaces and are more easily mobilised. Similar wettability-controlled transport behaviour has been reported in oil–water separation systems employing metallic meshes and porous substrates [43]. However, the present study demonstrates that highly effective selective behaviour can be achieved without relying on extreme superhydrophobic surface engineering, which is often associated with

poor mechanical durability and complicated fabrication routes. When integrated into porous metallic structures such as stainless steel meshes, the petroleum phase preferentially wets and permeates the surface. At the same time, water droplets are effectively repelled because of their non-wetting behaviour. Consequently, the pronounced shift from partial wetting in air to strong non-wetting behaviour in petroleum underscores the exceptional potential of the present Ni-based surfaces for high-performance petroleum–water separation applications.

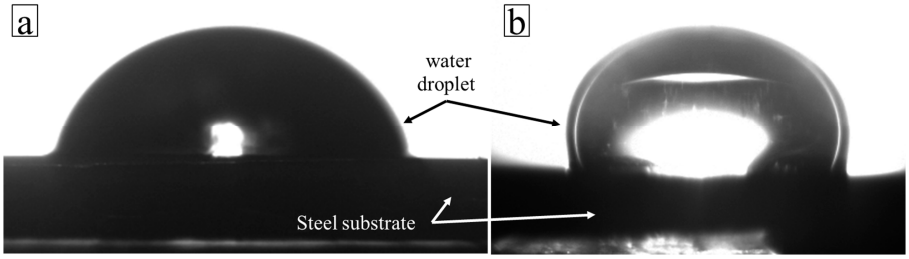


Figure 6. The silhouette of the water droplet on a stainless steel substrate surface ((**a**) in air, (**b**) under a petroleum phase).

3.2. The Ni Coating Investigation

The results of the Ni coating investigation show uniform coatings with a thickness of approximately 90 ± 10 nm (Figure 7). A uniform Ni coating ensures that the entire surface of the stainless steel mesh exhibits the same hydrophobic and oleophilic characteristics. This consistency is critical because any uncoated or unevenly coated areas could allow water to penetrate through the mesh, thereby reducing the overall separation efficiency. The uniform coating ensures that the entire mesh surface actively contributes to the separation process, optimising performance and ensuring that the mesh holes are evenly modified, maintaining a uniform hole size and shape and enabling better control over the passage of petroleum while blocking water. So, the nickel layer protects the underlying stainless steel from humidity and corrosive agents in the petroleum–water emulsion, maintaining mesh performance over time and preventing degradation under mechanical stress or during repeated separation cycles. The EDS analysis was used qualitatively to verify the presence and spatial distribution of Ni on different regions of the coated mesh surface.

3.3. The Measurement of the Contact Angle (CA) Without and with Ni Coating

3.3.1. Without Ni Coating

Based on the experimental results in Table 3, although the differences in wettability behaviour across all types of stainless steel mesh are insignificant, the effect of varying the number of meshes on liquid wettability is evident. The meshes were quickly wetted by petroleum in a second, while a distilled water droplet remained for a longer time without spreading or passing through the mesh with a contact angle of more than 106 ± 3°. Water droplets, being less viscous, can also coalesce or merge upon contact with the mesh, forming larger droplets that experience greater surface tension due to stronger cohesive forces among their molecules. At the same time, petroleum tends to spread out, cling to the mesh surface, and pass through it due to its reduced surface tension [49], thereby influencing its drift behaviour and interaction with the steel mesh. In addition, the metallic meshes used have a different hole size, engineered to be smaller than the dimensions of coalesced water droplets but larger than those of petroleum molecules.

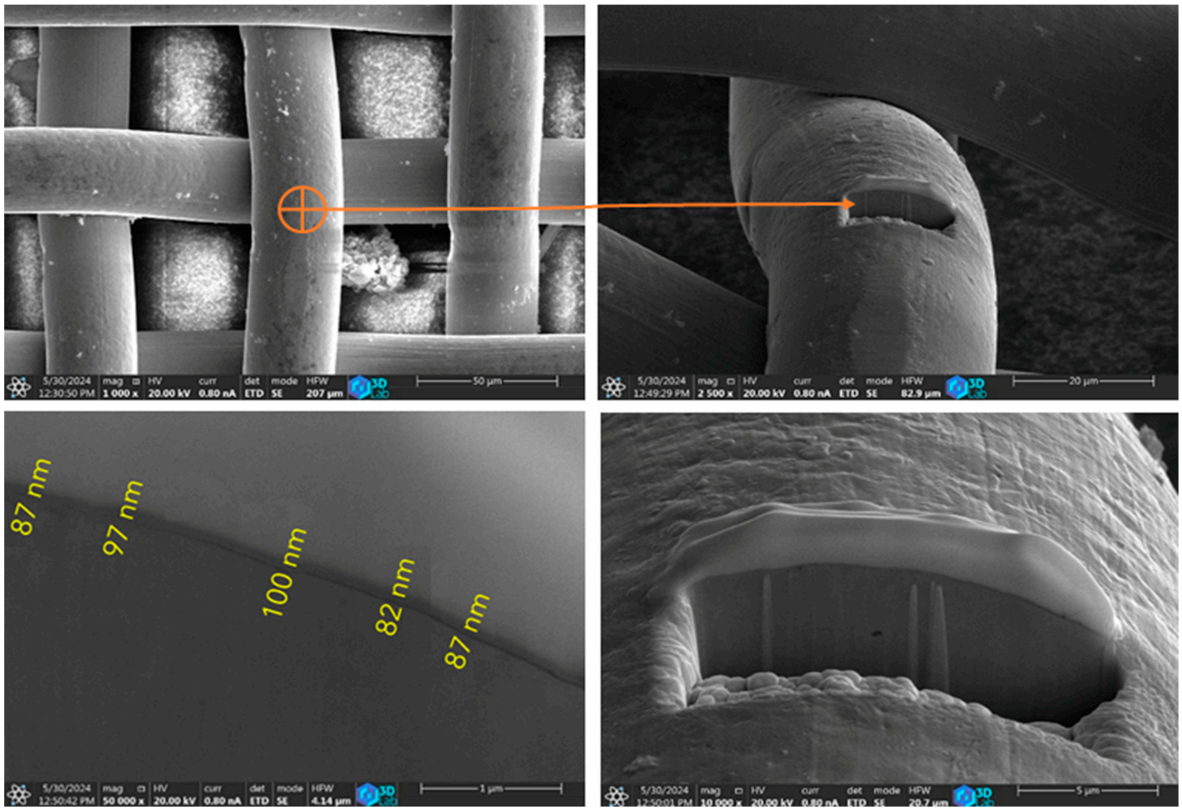


Figure 7. SEM image of the nickel coating thickness and position observation on the surface of stainless steel mesh wire (400 mesh size) using PFIB-SEM.

Table 3. The measured contact angle of the liquids on the stainless steel mesh surface without Ni coating.

	Liquids	Stainless Steel Mesh Size				
		500	**400**	**300**	**200**	**180**
Contact Angle θ° ± 3°	Petroleum	8	8	9	9	10
	Distilled water	129	121	115	110	106

When the petroleum droplet comes into contact with the stainless steel mesh, it spreads directly onto the surface. It passes through about 80% vol. through the mesh pores in just seconds, even as water droplets are captured and retained on the mesh surface, as seen in Figure 8. Surfaces with smaller hole sizes are smoother and less rough, which could decrease the petroleum contact angle. Still, when it is too large, it can cause water droplets to collapse, and the air in the large holes may no longer be confined. This layout offers a useful means to separate petroleum from water when the emulsion is applied to the mesh surface.

3.3.2. With Ni Coating

Based on the results in Table 4, the distilled water wetting slightly decreases as the Ni amount increases to twice the original amount with coating. In contrast, the petroleum maintains surface wetting with high-speed spreading. The improved petroleum wettability (lower petroleum contact angle) on the Ni-coated mesh is primarily attributed to the stronger affinity of nickel surfaces for hydrocarbons. Nickel readily promotes adsorption of petroleum components, forming a thin organic layer that enhances solid–petroleum interactions and lowers the solid–petroleum interfacial energy. As a result, petroleum spreads more easily on the Ni-coated surface. In contrast, the native oxide layer on uncoated stainless steel, which is more polar, provides a relatively weaker interaction with nonpolar petroleum, resulting in a higher petroleum contact angle.

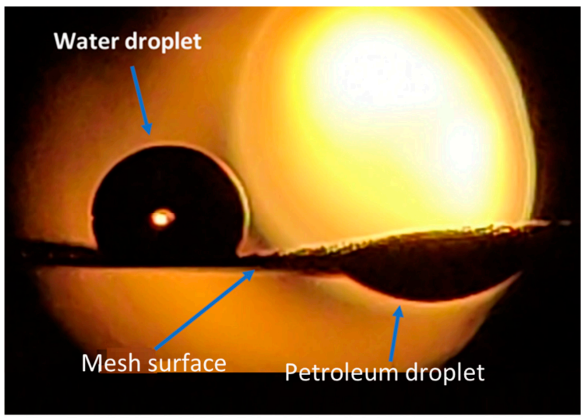


Figure 8. The silhouettes (after 1 min) of water and petroleum droplet wetting behaviour on the stainless steel mesh (400 mesh) surface with a Ni coating.

Table 4. The measured contact angle of the liquids on the stainless steel mesh surface with Ni coating.

	Liquids	Stainless Steel Mesh Size				
		500	**400**	**300**	**200**	**180**
Contact Angle θ° ± 3°	Petroleum	6	6	7	7	8
	Distilled water	131	123	118	112	110

Conversely, the higher water contact angle observed on the Ni-coated mesh indicates reduced water wettability due to two main effects: (i) the lower polarity of the nickel (and nickel oxide) surface compared to iron-rich oxides on stainless steel, and (ii) the adsorption of hydrophobic petroleum species, which reduces direct contact between water and the solid surface. These factors increase the solid–water interfacial energy and decrease the work of adhesion, leading to water droplets that bead up more on the Ni-coated surface. A decrease in petroleum flow was also observed as the stainless steel mesh size increased from 100 to 500 mesh, posing another challenge to the efficiency of the separation process.

3.4. The Calibration Measurements Description

To identify the efficiency of the separation in Section 3.5, a calibration line was prepared using the known mixtures prepared from Section 2.2.2, point a, and the investigation process in Section 2.4. The results showed a linear relationship (Figure 9) between the carbon content of petroleum and its percentage in the emulsion. The highest level of petroleum purity is achieved at a carbon content of 81% wt.

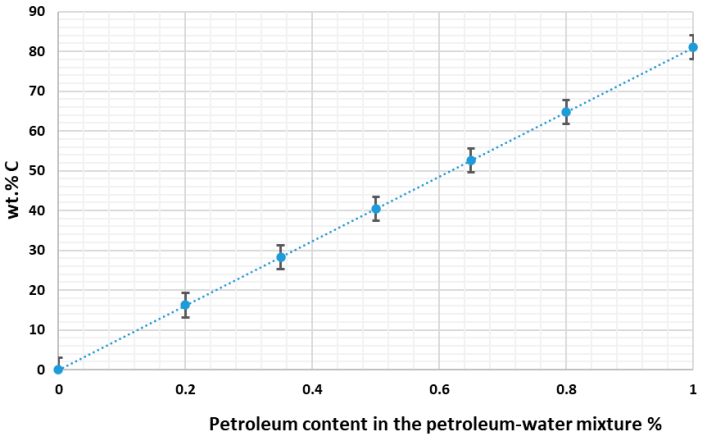


Figure 9. Calibration curve of the carbon content in the petroleum–water mixture.

3.5. The Petroleum–Water Emulsion Separation Efficiency

To determine the emulsion separation efficiency percentage using stainless steel meshes coated and uncoated with Ni, the average carbon weight percentages were quantified by the elemental analyser device and plotted on the y-axis for each mesh size; a horizontal projection was then drawn from the measured carbon weight persentage value to intersect the previously established calibration curve (see Section 3.4, Figure 9) obtained from mixtures with known petroleum–water compositions. From the intersection point, a vertical projection onto the x-axis was used to obtain the corresponding petroleum percentage. Higher carbon content values corresponded to higher petroleum purity in the separated liquid, as shown in Figures 10 and 11. Similar elemental analysis-based approaches have been used to evaluate oil–water separation efficiency due to their high sensitivity and quantitative reliability for determining hydrocarbon concentrations in multiphase systems [50].

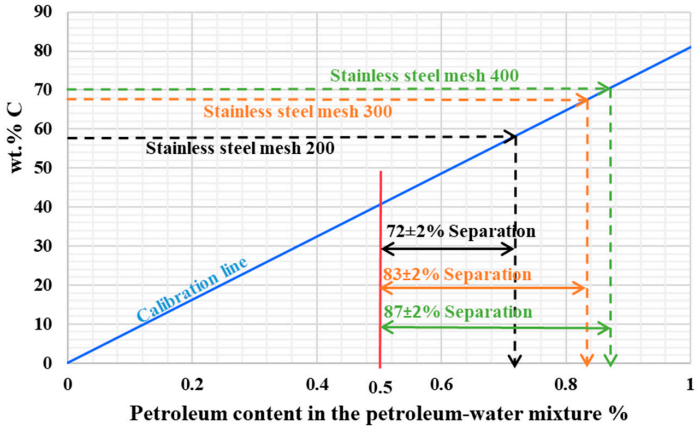


Figure 10. Identification of the C content for the separated liquid by the stainless steel meshes without Ni coating, with the C content for the initial emulsion (50% vol. petroleum + 50% vol. water); see the vertical red line in the figure.

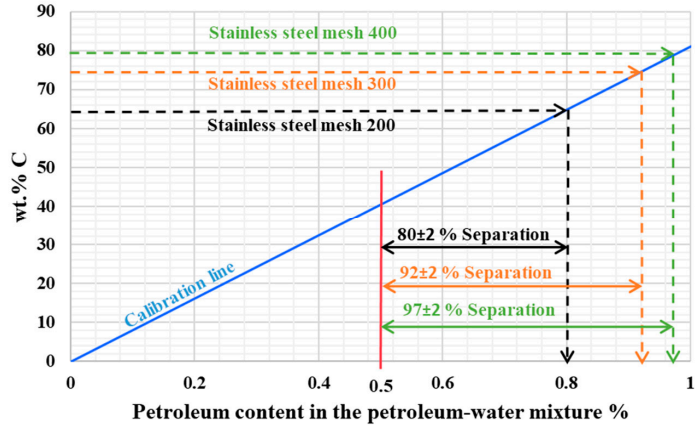


Figure 11. Identification of the C content for the separated liquid by the stainless steel meshes with Ni coating, with the C content for the initial emulsion (50% vol. petroleum + 50% vol. water); see the vertical red line in the figure.

The separation results show the superiority of mesh size (400 meshes), which demonstrated the highest rate of hydrophobicity and oleophilicity; the finer pore size and uniform Ni coating contributed to the superior separation of petroleum from water with 97 ± 2%. This excellent performance can be attributed to the combined effects of the finer pore structure and the highly uniform nanoscale Ni coating produced by the PVD process, both of which enhanced selective interfacial interactions during emulsion transport. The

efficiency obtained is highly competitive with, and in several cases superior to, previously reported coated metallic mesh systems, in which separation efficiencies generally range between 90% and 96% for conventional oil–water emulsions [9,51]. Although some advanced superhydrophobic systems have reported efficiencies approaching 99%, these often require complex hierarchical nanostructures, fluorinated chemical treatments, or multistep fabrication methods [50,52]. In contrast, the present work achieves near-comparable separation performance with a relatively simple, scalable PVD-deposited Ni coating, without requiring extreme surface modification or fluorinated compounds.

The enhanced separation behaviour can also be explained by the interfacial transport dynamics of the petroleum and water phases on the coated mesh surface. Water droplets, being less viscous, can also coalesce or merge when they come into contact with the mesh surface, forming larger droplets that increase surface tension due to stronger cohesive forces among their molecules. This droplet coalescence reduces water permeation through the mesh pores and promotes water rejection. Similar coalescence-driven separation mechanisms have been widely observed in metallic and membrane-based oil–water separation systems [53,54]. Conversely, petroleum spreads more readily across the Ni-coated surface due to its lower surface tension and greater affinity for the oleophilic coating, thereby facilitating selective permeation through the mesh. This preferential petroleum transport behaviour agrees well with previous wettability-driven separation models reported for metallic meshes and porous membranes [9,52].

The separation ratio for the 300 mesh stainless steel mesh also improved substantially after Ni coating, increasing to approximately 92 $\pm$ 2%, whereas the 200 mesh sample exhibited only a moderate improvement from 72 $\pm$ 2% (without Ni coating) to 80 $\pm$ 2% (with Ni coating). These findings indicate that mesh geometry plays a critical role in separation efficiency, alongside surface chemistry. Previous investigations have similarly demonstrated that pore size distribution strongly affects emulsion transport, capillary pressure, and selective phase permeation in oil–water separation systems [20,55]. The superior performance of the 300 and 400 mesh samples suggests that the finer pore structures provide greater capillary resistance to water penetration while maintaining continuous petroleum transport pathways.

The enhanced separation efficiency after Ni coating is attributed to modifications in the surface wettability and surface energy characteristics of the stainless steel meshes. The deposited Ni/NiO coating generated micro- and nanoscale surface features that enhanced selective wettability in accordance with the Wenzel and Cassie–Baxter wetting models. Similar wettability enhancement mechanisms have been extensively reported for textured metallic surfaces used in oil–water separation applications. Furthermore, the relatively lower polarity of nickel and nickel oxide surfaces, combined with the adsorption of hydrophobic petroleum species, reduces direct interaction between water and the solid surface. Therefore, it increases the solid–water interfacial energy and decreases the work of adhesion, leading to stronger bead formation on the coated surface. Comparable adsorption-induced wettability transitions have been reported for nickel-coated and hydrocarbon-exposed metallic substrates [45,46].

In addition, the uniform nanoscale coating (90 $\pm$ 10 nm) produced by the PVD process likely improved the consistency of overall wettability across the mesh surface and enhanced interfacial selectivity during emulsion separation. Uniform coatings minimise local wetting defects and provide more homogeneous phase interactions across the mesh surface. Several studies have shown that coating uniformity and nanoscale roughness strongly influence emulsion separation performance and long-term wetting stability [50,55]. These combined effects explain why the Ni-coated meshes achieved higher separation efficiencies, particularly for the 300 and 400 mesh samples.

Notably, the present work demonstrates that measurable and highly effective emulsion separation can still be achieved using a relatively simple nanoscale Ni coating deposited by PVD, even without achieving classical superhydrophobic behaviour. This finding is particularly important because many previously published studies [35,56,57] have mainly focused on achieving extreme wetting behaviour, such as superhydrophobicity or underwater superoleophobicity, through complex nanostructured or chemically modified coatings using sophisticated nanostructuring, fluorinated modifications, laser texturing, or chemical etching techniques.

On the other hand, comparing the separation efficiencies of all coated and uncoated mesh samples (Figure 12) revealed that the 180 and 500 mesh samples exhibited inferior separation performance. The 180 mesh sample produced poor separation efficiency (58 ± 2%) because the relatively large pore openings allowed portions of the emulsion to pass directly through the mesh without effective phase discrimination. Similar decreases in efficiency for excessively large pore structures have been reported previously in porous metallic separators and membrane systems [20]. Conversely, the 500 mesh sample exhibited slow separation kinetics and a reduced separation efficiency below 66 ± 2%, likely due to its extremely fine pore structure, which restricted petroleum permeation and increased flow resistance. This behaviour agrees with previously reported observations that excessively small pore sizes can hinder flux and delay emulsion transport despite improved capillary resistance [51,55]. Therefore, the 400 mesh and 300 mesh sizes appear to provide an optimal balance between selective permeation and transport rate.

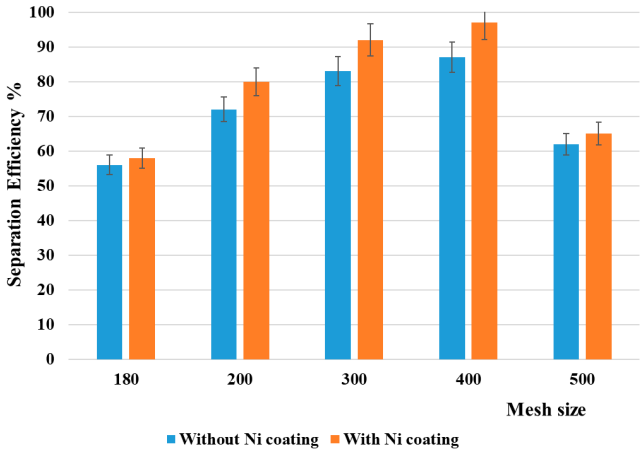


Figure 12. Influence of stainless steel mesh size on the efficiency of emulsion separation with and without Ni coating.

The present work further suggests that efficient petroleum–water separation may occur under moderate wettability conditions, even without generating superhydrophobic surfaces. This observation differs from many published studies [50–52] that associate high separation performance exclusively with contact angles exceeding 150°. Therefore, broadens understanding that effective petroleum–water separation is not governed solely by extreme contact angles, but rather by the combined influence of surface chemistry, interfacial interactions, pore geometry, and emulsion transport behaviour. This conclusion may have important practical implications because moderately wetting systems are often mechanically more stable and easier to fabricate than extremely superhydrophobic surfaces, which frequently suffer from durability and contamination issues during long-term operation [53].

Although the present study did not include a quantitative lifetime evaluation, the Ni coating is expected to improve the operational lifespan of the stainless steel meshes by

acting as a protective barrier against corrosive species present in petroleum–water emulsions as a result of the chemical stability of Ni coatings reported in previous studies [58], the uniformity of the deposited coating observed by SEM/EDS, and the stable separation performance during repeated experimental cycles. Unlike some highly engineered nanostructured systems that require complex multistep fabrication routes, the present study uses commercially available stainless steel meshes and a conventional PVD coating process, which may offer practical advantages in scalability, mechanical durability, and low-cost industrial implementation.

4. Conclusions

In this study, the efficiency of petroleum–water separation was evaluated by applying the emulsion to a range of distinct stainless steel mesh sample sizes (500, 400, 300, 200, and 180 meshes) without and with being coated with 0.10 μm of Ni by the PVD technique. The findings are as follows:

- The Ni-coated meshes achieved high petroleum–water separation efficiencies of 97 ± 2% and 92 ± 2% for the 400 and 300 mesh sizes, respectively, using a relatively simple nanoscale Ni coating deposited via conventional PVD without the need for fluorinated chemicals, expensive nanomaterials, or multilayer coatings.
- The improved oil–water separation efficiency achieved by the Ni-coated meshes may help reduce water transport to downstream equipment under moderate wettability conditions, even without the formation of superhydrophobic surfaces, when pore geometry, interfacial selectivity, capillary behaviour, and transport dynamics are properly controlled, potentially lowering corrosion risk in industrial systems.
- The separation efficiency and stability after repeated use demonstrate their mechanical stability and reusability. It highlights the dual functionality of the Ni coating, which improves selective wettability and may enhance corrosion resistance and operational durability.
- The use of a stainless steel mesh coated with Ni could eliminate the need for chemical surfactants or fluorinated compounds, reducing environmental impact.
- The precision of mesh size identification is an important parameter that could affect the separation efficiency. The results showed a different range of separation efficiency across mesh sizes, with 200 mesh increasing from 72 ± 2% without coating to 80 ± 2% with coating, while 180 and 500 mesh reached 58 ± 2% and 66 ± 2%, respectively.
- Although the increase in water contact angle under petroleum and the improved separation efficiency suggest enhanced selective wettability, the interfacial separation mechanism is likely influenced by additional factors such as surface energy, surface roughness, pore geometry, and emulsion droplet interactions.

Author Contributions: Conceptualization, M.K. and P.B.; Methodology, M.K. and P.B.; Validation, M.K.; Investigation, M.K.; Data curation, M.K. and P.B.; Writing—original draft, M.K.; Writing—review & editing, P.B.; Visualization, P.B.; Supervision, P.B. All authors have read and agreed to the published version of the manuscript.

Funding: This research received no external funding.

Data Availability Statement: The original contributions presented in this study are included in the article. Further inquiries can be directed to the corresponding authors.

Acknowledgments: The authors would like to express their sincere gratitude to the TEMPUS Public Foundation and the Stipendium Hungaricum Scholarship for their support, as well as to the University of Miskolc, particularly the Institute of Physical Metallurgy, Metal Forming, and Nanotechnology, for kindly providing their laboratories. The invaluable support from the University has greatly contributed to the success of this research work.

Conflicts of Interest: Author Mohanad Khairi was employed by the Inspection Engineering Department, Midland Oil Company, Ministry of Oil. The remaining authors declare that the research was conducted in the absence of any commercial or financial relationships that could be construed as a potential conflict of interest.

References

1. Zhang, H.; Lan, H.Q. A review of internal corrosion mechanism and experimental study for pipelines based on multiphase flow. *Corros. Rev.* **2017**, *35*, 425–444. [CrossRef]
2. Askari, M.; Aliofkhazraei, M.; Afroukhteh, S. A comprehensive review on internal corrosion and cracking of oil and gas pipelines. *J. Nat. Gas Sci. Eng.* **2019**, *71*, 102971. [CrossRef]
3. Shabarchin, O.; Tesfamariam, S. Internal corrosion hazard assessment of oil & gas pipelines using Bayesian belief network model. *J. Loss Prev. Process Ind.* **2016**, *40*, 479–495. [CrossRef]
4. Eliyan, F.F.; Gadala, I.M.; Ha, H.; Alfantazi, A. Chapter 42 | Corrosion of Pipeline Steel. In *Fuels and Lubricants Handbook: Technology, Properties, Performance, and Testing*; Totten, G.E., Shah, R.J., Forester, D.R., Eds.; ASTM International: West Conshohocken, PA, USA, 2019. [CrossRef]
5. Kareem, M.Q.; Miko, T.; Gergely, G.; Gacsi, Z. A review on the production of 17-4PH parts using press and sinter technology. *Sci. Prog.* **2023**, *106*. [CrossRef]
6. de Freitas, D.S.; da Silva, C.A.M.; Gonçalves, I.L.M. Mechanisms of corrosion of pipelines. In *Handbook of Pipeline Engineering*; Springer International Publishing: Cham, Switzerland, 2023; pp. 1–40.
7. Ni, Y.; Xu, Z.; Zhang, X.; Yin, H.; Li, T.; Hu, C. A robust superhydrophobic-superoleophilic stainless steel mesh with superior mechanical durability and chemical stability for oil-water separation. *Surf. Interfaces* **2025**, *66*, 106578. [CrossRef]
8. Omidali, F.; Azizian, S.; Sohrabi, B.; Shabanlou, E.; Jaleh, B. Fabrication of highly-hydrophobic steel meshes using pulsed laser ablation and surface modification methods for oil/water separation. *Surf. Interfaces* **2025**, *64*, 106402. [CrossRef]
9. Xue, Z.; Cao, Y.; Liu, N.; Feng, L.; Jiang, L. Special wettable materials for oil/water separation. *J. Mater. Chem. A* **2014**, *2*, 2445–2460. [CrossRef]
10. Yu, J.; Cao, C.; Pan, Y. Advances of adsorption and filtration techniques in separating highly viscous crude oil/water mixtures. *Adv. Mater. Interfaces* **2021**, *8*, 2100061. [CrossRef]
11. Mohanad, K.; Zoltán, E.; Peter, B. Wettability of Polar and Apolar Liquids on Metal Surfaces. *Metals* **2024**, *15*, 23. [CrossRef]
12. Zhu, M.; Liu, Y.; Chen, M.; Xu, Z.; Li, L.; Zhou, Y. Metal mesh-based special wettability materials for oil-water separation: A review of the recent development. *J. Pet. Sci. Eng.* **2021**, *205*, 108889. [CrossRef]
13. Zhang, L.; Zhang, Z.; Wang, P. Smart surfaces with switchable superoleophilicity and superoleophobicity in aqueous media: Toward controllable oil/water separation. *NPG Asia Mater.* **2012**, *4*, e8. [CrossRef]
14. Kumari, P.; Poonam, C.; Aditya, K. Superwetting materials for modification of meshes for oil/water separation. In *Oil−Water Mixtures and Emulsions, Volume 2: Advanced Materials for Separation and Treatment*; American Chemical Society: Washington, DC, USA, 2022; pp. 1–23.
15. Xue, Z.; Wang, S.; Lin, L.; Chen, L.; Liu, M.; Feng, L.; Jiang, L. A novel superhydrophilic and underwater superoleophobic hydrogel-coated mesh for oil/water separation. *Adv. Mater.* **2011**, *37*, 4270–4273. [CrossRef]
16. Wen, Q.; Di, J.; Jiang, L.; Yu, J.; Xu, R. Zeolite-coated mesh film for efficient oil–water separation. *Chem. Sci.* **2013**, *4*, 591–595. [CrossRef]
17. Li, B.; Qian, X.; Ran, L.; Han, J.; Yang, C.; Jiao, T. Applications and challenges of superwetted oil-water separation membranes in air under liquids and in specific environments. *Prog. Org. Coat.* **2024**, *195*, 108673. [CrossRef]
18. Sun, Y.; Ke, Z.; Shen, C.; Wei, Q.; Sun, R.; Yang, W.; Yin, Z. Facile Construction and Fabrication of a Superhydrophobic and Super Oleophilic Stainless Steel Mesh for Separation of Water and Oil. *Nanomaterials* **2022**, *12*, 1661. [CrossRef]
19. Melnik, A.; Bogoslovtseva, A.; Petrova, A.; Safonov, A.; Markides, C.N. Oil–water separation on hydrophobic and superhydrophobic membranes made of stainless steel meshes with fluoropolymer coatings. *Water* **2023**, *15*, 1346. [CrossRef]
20. Myeong, J.; Deshmukh, P.R.; Shin, W.G. Facile preparation of superhydrophilic and underwater superoleophobic stainless steel mesh for oil–water separation. *J. Ind. Eng. Chem.* **2023**, *120*, 398–409. [CrossRef]
21. Liu, K.; Jiang, L. Metallic surfaces with special wettability. *Nanoscale* **2011**, *3*, 825–838. [CrossRef] [PubMed]
22. Li, C.; Li, N.; Zhang, X.; Dong, Z.; Chen, H.; Jiang, L. Uni-directional transportation on peristome-mimetic surfaces for completely wetting liquids. *Angew. Chem. Int. Ed.* **2016**, *55*, 14988–14992. [CrossRef]
23. Wang, B.; Guo, Z. Superhydrophobic copper mesh films with rapid oil/water separation properties by electrochemical deposition inspired from butterfly wing. *Appl. Phys. Lett.* **2013**, *103*, 063704. [CrossRef]
24. Chen, Q.; de Leon, A.; Advincula, R.C. Inorganic–organic thiol–ene coated mesh for oil/water separation. *ACS Appl. Mater. Interfaces* **2015**, *7*, 18566–18573. [CrossRef]

25. Wang, B.; Li, J.; Wang, G.; Liang, W.; Zhang, Y.; She, L.; Guo, Z.; Liu, W. Methodology for robust superhydrophobic fabrics and sponges from in situ growth of transition metal/metal oxide nanocrystals with thiol modification and their applications in oil/water separation. *ACS Appl. Mater. Interfaces* **2013**, *5*, 1827–1839. [CrossRef]
26. Zhang, J.; Seeger, S. Polyester materials with superwetting silicone nanofilaments for oil/water separation and selective oil absorption. *Adv. Funct. Mater.* **2011**, *21*, 4699–4704. [CrossRef]
27. Vandchali, H.R.; Peyravi, M.; Yekani, N.H. Ni modified superhydrophobic mesh membranes with flower-like hierarchical structure for oil/water separation. *Surf. Interfaces* **2025**, *78*, 108132. [CrossRef]
28. Wang, Y.; Liu, P.; Luo, R.; Chen, B.; Li, J.; Yang, F.; Zhou, H.; Zeng, J.; Xing, L.; Guo, J. Design and fabrication of superhydrophobic photothermal coating on copper mesh and its applications on anti-corrosion, anti-icing and oil-water separation. *Prog. Org. Coat.* **2024**, *188*, 108243. [CrossRef]
29. Deachophon, A.; Bovornratanaraks, T.; Poompradub, S. Modified silica-based double-layered hydrophobic-coated stainless steel mesh and its application for oil/seawater separation. *Sci. Rep.* **2024**, *14*, 731. [CrossRef]
30. Li, B.; Liu, X.; Zhang, X.; Chai, W. Stainless steel mesh coated with silica for oil–water separation. *Eur. Polym. J.* **2015**, *73*, 374–379. [CrossRef]
31. Kang, H.; Sun, Y.; Li, Y.; Qin, W.; Wu, X. Mechanically robust fish-scale microstructured TiO_2-coated stainless steel mesh by atomic layer deposition for oil–water separation. *Ind. Eng. Chem. Res.* **2020**, *59*, 21088–21096. [CrossRef]
32. Myeong, S.; Lim, C.; Kim, S.; Lee, Y.S. High-efficiency oil/water separation of hydrophobic stainless steel Mesh filter through carbon and fluorine surface treatment. *Korean J. Chem. Eng.* **2023**, *40*, 1418–1424. [CrossRef]
33. Becker, R. Die Keimbildung bei der Ausscheidung in metallischen Mischkristallen. *Ann. Phys.* **1938**, *424*, 128–140. [CrossRef]
34. Nishizawa, T.; Ohnuma, I.; Ishida, K. Correlation between interfacial energy and phase diagram in ceramic-metal systems. *J. Phase Equilibria* **2001**, *22*, 269–275. [CrossRef]
35. Gao, Q.; Li, J.; Ma, R.; Fan, Y.; Du, A.; Yang, M.; Zhao, X.; Bian, Y. Facile electrodeposition of corrosion-resistant superhydrophobic Ni-plated stainless-steel mesh for oil–water separation. *Mater. Today Commun.* **2023**, *37*, 107032. [CrossRef]
36. Zhang, X.; Hu, C.; Fu, X.; Zhang, S.; Li, T.; Ma, B.; Ren, K. An ultra-thin nickel electrodeposited stainless steel mesh with superhydrophobic property and high mechanical durability for oil-water separation. *J. Environ. Chem. Eng.* **2024**, *12*, 111692. [CrossRef]
37. Zhang, W.; Hu, C.; Bai, C.; Zhang, X.; Zhang, S.; Tang, J.; Kong, Y.; Li, T. A rapid two-step process to prepare a high-throughput, efficient, reusable superhydrophobic–superoleophilic stainless steel mesh for oil/water separation. *J. Adhes. Sci. Technol.* **2024**, *38*, 2557–2583. [CrossRef]
38. Sreekumar, R.; Thazhakkuni, S.E.; Suseelamma, S.S. Fabrication of a robust superhydrophobic stainless steel mesh for efficient oil/water separation. *J. Ind. Eng. Chem.* **2024**, *135*, 425–433. [CrossRef]
39. Liu, P.; Wu, L.; Guo, Y.; Huang, X.; Guo, Z. Rapid preparation of Ni/Fe-LDH@ stainless steel mesh with interfacial emulsion breaking effect for efficient oil-in-water emulsion separation. *Colloids Surf. A Physicochem. Eng. Asp.* **2024**, *681*, 132792. [CrossRef]
40. Hou, Y.; Li, R.; Liang, J. Superhydrophilic nickel-coated meshes with controllable pore size prepared by electrodeposition from deep eutectic solvent for efficient oil/water separation. *Sep. Purif. Technol.* **2018**, *192*, 21–29. [CrossRef]
41. Somlyai-Sipos, L.; Baumli, P. Wettability of Metals by Water. *Metals* **2022**, *12*, 1274. [CrossRef]
42. Eslamibidgoli, M.J.; Groß, A.; Eikerling, M. Surface configuration and wettability of nickel (oxy) hydroxides: A first-principles investigation. *Phys. Chem. Chem. Phys.* **2017**, *19*, 22659–22669. [CrossRef]
43. Qian, X.; Tang, T.; Wang, H.; Chen, C.; Luo, J.; Luo, D. Fabrication of hydrophobic Ni surface by chemical etching. *Materials* **2019**, *12*, 3546. [CrossRef]
44. Frieder, M.; Bijoyendra, B.; Andrea, C.; Igor, S.; Armando, M.; Michel, D.; Martien, C.; van den, E.D.; Isabella, S.; Ian, C. Ion adsorption-induced wetting transition in oil-water-mineral systems. *Sci. Rep.* **2015**, *5*, 10519. [CrossRef]
45. Artur, P.T.; Paweł, B.; Emil, K.; Piotr, K.; Anna, Z.; Przemysław, P.; Marek, W.; Radosław, P.W. Water nanodroplet on a hydrocarbon "carpet"—The mechanism of water contact angle stabilisation by airborne contaminations on graphene, Au, and PTFE surfaces. *Langmuir* **2018**, *35*, 420–427. [CrossRef]
46. Standal, S.; Haavik, J.; Blokhus, A.M.; Skauge, A. Effect of polar organic components on wettability as studied by adsorption and contact angles. *J. Pet. Sci. Eng.* **1999**, *24*, 131–144. [CrossRef]
47. Starkweather, B.A.; Zhang, X.; Counce, R.M. An experimental study of the change in the contact angle of an oil on a solid surface. *Ind. Eng. Chem. Res.* **2000**, *39*, 362–366. [CrossRef]
48. Setiawan, I.; Trisnanto, S.R.; Suryani, I.O. Dynamic contact angle and corrosion test measurements on Cu and CuO-stearic acid modifications on steel surfaces. *Indones. J. Comput. Eng. Des. (IJoCED)* **2020**, *2*, 49–57. [CrossRef]
49. Zhang, Y.P.; Wang, Y.N.; Wan, L.; Chen, X.X.; Zhao, C.H. Superwetting stainless steel mesh used for both immiscible oil/water and surfactant-stabilised emulsion separation. *Membranes* **2023**, *13*, 808. [CrossRef]
50. Liu, K.; Cao, M.; Fujishima, A.; Jiang, L. Bio-inspired titanium dioxide materials with special wettability and their applications. *Chem. Rev.* **2014**, *114*, 10044–10094. [CrossRef]

51. Chu, Z.; Feng, Y.; Seeger, S. Oil/water separation with selective superantiwetting/superwetting surface materials. *Angew. Chem. Int. Ed.* **2015**, *54*, 2328–2338. [CrossRef]
52. Yong, J.; Chen, F.; Yang, Q.; Bian, H.; Du, G.; Shan, C.; Huo, J.; Fang, Y.; Hou, X. Oil-Water Separation: A Gift from the Desert. *Adv. Mater. Interfaces* **2016**, *3*, 1500650. [CrossRef]
53. Gregory, D.B.; Bharat, B. Bioinspired rice leaf and butterfly wing surface structures combining shark skin and lotus effects. *Soft Matter* **2012**, *8*, 11271–11284. [CrossRef]
54. Arun, K.K.; Yongxin, L.; Joseph, M.M.; Anish, T. Hierarchically structured superoleophobic surfaces with ultralow contact angle hysteresis. *Adv. Mater.* **2012**, *24*, 5838–5843. [CrossRef] [PubMed]
55. Wang, B.; Liang, W.; Guo, Z.; Liu, W. Biomimetic super-lyophobic and super-lyophilic materials applied for oil/water separation: A new strategy beyond nature. *Chem. Soc. Rev.* **2015**, *44*, 336–361. [CrossRef] [PubMed]
56. Zhang, Y.; Wang, H.; Liu, B.; Zhao, X.; Wei, Y. $NiCo_2O_4$ hierarchical structure coated mesh with long-term stable underwater superoleophobicity for high-efficient, high-flux oil-water separation. *Appl. Surf. Sci.* **2020**, *504*, 144598. [CrossRef]
57. Mahmodi, G.; Dangwal, S.; Zarrintaj, P.; Zhu, M.; Mao, Y.; Mcllroy, D.N.; Saeb, M.R.; Vatanpour, V.; Ramsey, J.D.; Kim, S.J. NaA zeolite-coated meshes with tunable hydrophilicity for oil-water separation. *Sep. Purif. Technol.* **2020**, *240*, 116630. [CrossRef]
58. Low, C.T.J.; Wills, R.G.A.; Walsh, F.C. Electrodeposition of composite coatings containing nanoparticles in a metal deposit. *Surf. Coat. Technol.* **2006**, *201*, 371–383. [CrossRef]

Disclaimer/Publisher's Note: The statements, opinions and data contained in all publications are solely those of the individual author(s) and contributor(s) and not of MDPI and/or the editor(s). MDPI and/or the editor(s) disclaim responsibility for any injury to people or property resulting from any ideas, methods, instructions or products referred to in the content.